Organic & Biomolecular Chemistry

PAPER

View Article Online
View Journal | View Issue

Cite this: *Org. Biomol. Chem.*, 2014, **12**, 5235

Outstanding effects on antithrombin activity of modified TBA diastereomers containing an optically pure acyclic nucleotide analogue†

M. Scuotto,‡ M. Persico,‡ M. Bucci, V. Vellecco, N. Borbone, E. Morelli, G. Oliviero, E. Novellino, G. Piccialli, G. Cirino, M. Varra,* C. Fattorusso* and L. Mayol

Received 20th January 2014,
Accepted 16th May 2014

DOI: 10.1039/c4ob00149d

www.rsc.org/obc

Herein, we report optically pure modified acyclic nucleosides as ideal probes for aptamer modification. These new monomers offer unique advantages in exploring the role played in thrombin inhibition by a single residue modification at key positions of the TBA structure.

Introduction

Aptamers are short, structured, single-stranded RNA or DNA ligands characterized by high affinity and specificity for their target molecules. Aptamers can be considered as oligonucleotide analogs of antibodies,[1,2] but, unlike antibodies, they can be chemically derivatized to extend their lifetimes and/or their bioavailability[3,4] and, particularly, to explore the molecular basis of their biological properties.[5,6] The thrombin binding aptamer (TBA) is a 15-mer oligonucleotide (ON) which folds into a typical chair-like G-quadruplex structure containing one TGT and two TT loops (Fig. 1).[7–9] It binds thrombin acting as an anticoagulant agent.[10]

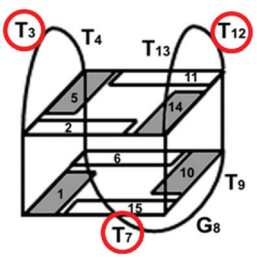

Fig. 1 Schematic representation of the NMR derived structure of TBA. White and black rectangles indicate G bases in *anti* and *syn* conformation, respectively. Loop residues not stacked on the G tetrads are highlighted by red circles.

Dipartimento di Farmacia, via D. Montesano 49, 80131 Napoli, Italy.
E-mail: varra@unina.it, cfattoru@unina.it; Fax: +39 081678552; Tel: +39 081678540, +39 081678544

† Electronic supplementary information (ESI) available: Fig. S1–S3 and Tables S1 and S2. See DOI: 10.1039/c4ob00149d

‡ These authors equally contributed to this work.

The investigation of the complex and intriguing molecular bases of TBA–thrombin interactions has lasted now for more than two decades.[11–14] There is a certain amount of knowledge[4,8,9,11–15] on the fact that TBA loops are fundamental for both G-quadruplex folding and thrombin interaction. In TBA experimentally determined structures, either alone[8,9] or in complex with thrombin,[11–14] the TT loops always preserved the same conformation, having T4 and T13 stacked on the underlying G quartet and T3 and T12 available for thrombin interaction. In contrast, the TGT loop showed higher conformational flexibility, especially concerning the T7 residue, which is reported to interact with thrombin in some X-ray complexes.[11,12] Previous structure–activity relationship (SAR) studies on TBA analogues containing an acyclic nucleotide, performed by us[16,17] and others,[18,19] confirmed that some loop residues, specifically T4, T13, G8, and T9, are crucial to preserve the G-quadruplex folding typology, whereas the others, T3, T12, and T7, are uniquely involved in thrombin inhibition. Indeed, ONs modified at T3, T12, and T7 showed significantly different biological behaviours with respect to TBA, not related to the stability of their G-quadruplex structure. We rationalized[17] the SARs obtained by substituting **a** or **b** (Fig. 2) at T3, T12, and T7, through enzyme-aptamer multiple binding modes (Fig. 3). Disadvantageously, since the introduced residues **a** or **b** presented a pro-chiral carbon (Fig. 2), each obtained modified sequence existed as a mixture of two diastereomers.

On this basis, the substitution of the identified key residues with a rationally designed and optically pure acyclic nucleoside analogue would allow the investigation of the molecular bases of TBA–thrombin interaction. Here, we successfully approach this issue by the substitution of T3 or T7 or T12 with each pure stereoisomer of the acyclic nucleoside **c** (Fig. 2).

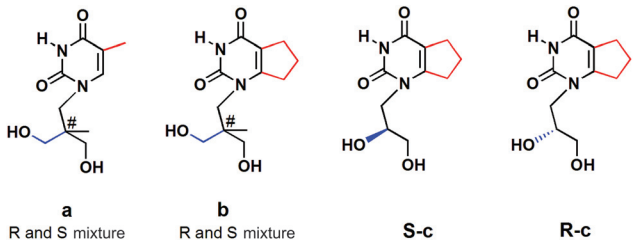

Fig. 2 Acyclic nucleosides mimicking thymine residues. The pro-chiral carbon of **a** and **b** is labelled with #.

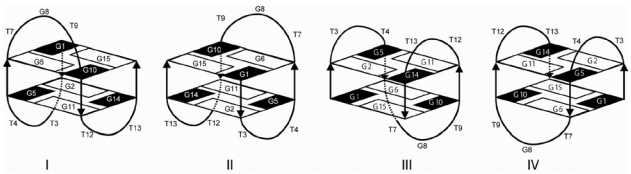

Fig. 3 Schematic representation of the four possible orientations of TBA with respect to thrombin assuming the same strand polarity of the X-ray complex. White and black rectangles indicate G bases in *anti* and *syn* conformation, respectively.

Results and discussion

Synthesis

We adopted the Horhota method[20] to obtain the stereoselective synthesis of *R* and *S* enantiomers of the acyclic nucleoside **c** (**R-c** and **S-c** in Scheme 1, Fig. 2 and Fig. 4). The *R* or *S* stereochemistry was attained by ring opening of the enantiomerically pure chiral epoxides **2** by reaction with the modified nucleobase **1** (Scheme 1). Each achieved molecule was converted into the corresponding phosphoramidite building block (**5a,b**) and incorporated into the TBA sequence to obtain a pool of six ONs (Table 1).

Structural characterization

To probe whether the introduction of *R* or *S* acyclic nucleoside **c** at TBA position 3, 12 or 7 affected the overall G-quadruplex topology formed in solution, we characterized all modified TBAs by circular dichroism (CD) and CD melting experiments.

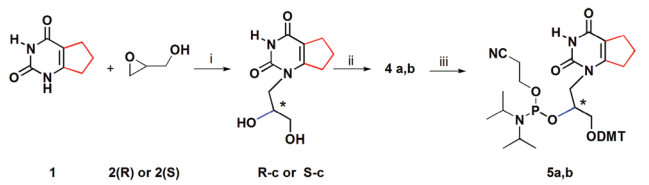

Scheme 1 Synthesis of monomers **5a,b**. (i) **1** 1.0 g (6.6 mmol), **2** (pure enantiomer *R* or *S*) 0.490 g (6.6 mmol), potassium carbonate 0.152 g (1.1 mmol), dry DMF (24 mL), 12–18 h, 80 °C, yields **R-c** 60% and **S-c** 45%; (ii) **R-c** or **S-c** 560 mg (2.5 mmol), 4,4′-dimethoxytritylchloride 850 mg (2.5 mmol), 4-dimethylaminopyridine 15 mg (0.12 mmol), pyridine (20 mL), 2.0 h, r.t., yields 85%; (iii) **4a,b** 859 mg, (1.6 mmol), 2-cyanoethyl diisopropylchlorophosphoramidite 536 μL (2.4 mmol), DIPEA 1.7 mL (10 mmol), DCM (9 mL), 40 min, r.t., yields 90%.

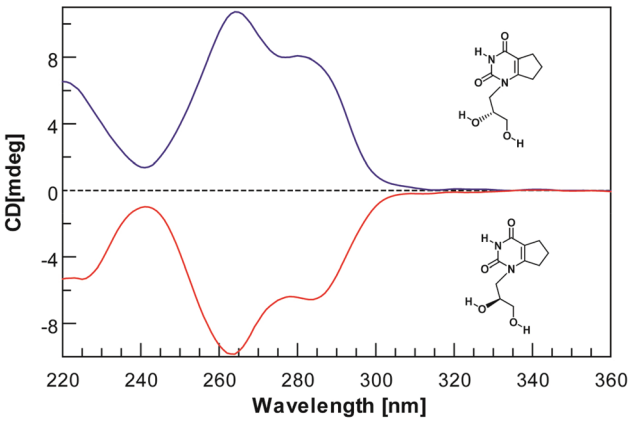

Fig. 4 CD spectra of modified acyclic nucleosides (3.6×10^{-4} M in CH_3OH) **R-c** (positive spectrum) and **S-c** (negative spectrum).

Table 1 Modified sequences containing the **c** derivatives instead of a T residue. The incorporation of **R-c** or **S-c** stereoisomer was specified substituting, at each position, the letter T of the unmodified sequence for the letter **R** or **S**, respectively

ON	Sequence
TBA	GGTTGGTGTGGTTGG
TBA-R_{12}	GGTTGGTGTGG**R**$_{12}$TGG
TBA-R_3	GG**R**$_3$TGGTGTGGTTGG
TBA-R_7	GGTTGG**R**$_7$GTGGTTGG
TBA-S_7	GGTTGG**S**$_7$GTGGTTGG
TBA-S_{12}	GGTTGGTGTGG**S**$_{12}$TGG
TBA-S_3	GG**S**$_3$TGGTGTGGTTGG

As expected, in PBS and K^+ (90 mM KCl, 10 mM K_2HPO_4, pH = 7.3) buffers, the modified sequences fold into G-quadruplexes having CD profiles (Fig. 5) and apparent melting temperatures (Table 2 and Fig. S1 in ESI†) comparable to that of TBA. Particularly, a stabilizing effect on the G-quadruplex structure (ΔT = 4–5 °C) was attained by replacing the T residue

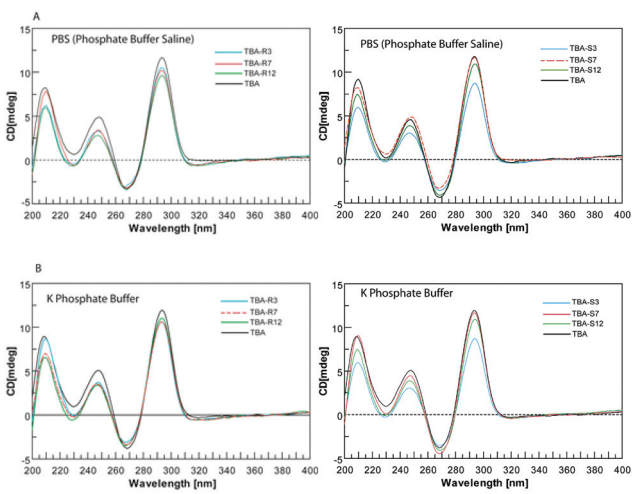

Fig. 5 CD spectra of TBA and modified ONs in PBS (A) and K^+ phosphate buffer (B).

Table 2 T_m values of TBA and modified ONs

	T_m °C (±1.0 °C)	
ON	K^+	PBS
TBA	50	34
TBA-R_{12}	55	39
TBA-R_3	55	39
TBA-R_7	54	38
TBA-S_7	56	39
TBA-S_{12}	51	35
TBA-S_3	51	35

at positions 3 and 12 with the *R* stereoisomer of **c** or at position 7 with both the *R* and *S* stereoisomers.

Fibrinogen assay

The new ONs were then evaluated for their ability to inhibit fibrinogen hydrolysis by a fibrinogen clotting assay. The clotting of fibrinogen induced by human α-thrombin was measured spectrophotometrically at different aptamer concentrations, following the increase in absorbance at 380 nm as a function of time (Fig. 6 and 7, Table 3, Fig. S2 in ESI,† and Experimental section).

At 20 nM concentration, TBA and TBA-R_{12} prolonged the basal clotting time of 56 and 199 s, respectively (Fig. 6 and Table 3).

Thus, TBA-R_{12} was 3.5 fold more active than TBA. At the same concentration, TBA-S_{12} was completely inactive (Fig. 7 and Table 3). A similar activity trend was also observed between TBA-R_3 and TBA-S_3, the former being 1.9 fold more active than TBA, and the latter completely inactive (Fig. 6 and 7 and Table 3). These activity trends were maintained at all tested concentrations, thus evidencing a stereoselective interaction with the target, involving the modified T12 or T3 residues, which is crucial for thrombin inhibition.

Molecular modelling studies

The resulting SARs of the new modified ONs were rationalized with the aid of molecular modelling studies (see the Experimental section for details). As observed by Feigon *et al.*[8] and confirmed by X-ray data,[12,14] due to the TBA symmetry, residues T3 and T12 occupy equivalent positions with respect to the G quartets and, by consequence, their binding clefts at thrombin Exosite I (ABE I) can be "exchanged" by rotating the structure 180° around the *Y*-axis (binding modes III and IV in Fig. 3 and 8). Conversely, the TBA symmetry is lost when either T3 or T12 is modified and, in particular, TT loops are no longer equivalent. In our case, the monomer **c** is characterized by (i) higher conformational flexibility and (ii) greater steric hindrance with respect to thymidine. Our computational results indicated that TBA-R_3 and TBA-R_{12}, which preserved the stereochemistry of the thymidine residue, could easily adopt bioactive conformation of the TT loops (Fig. 9a). The significant increase in inhibitory activity of TBA-R_3 and TBA-R_{12} with respect to TBA indicates the presence of additional favourable hydrophobic contacts with the protein in, at least, one of the TT loop binding clefts. In contrast, when the stereochemistry of **c** is inverted with respect to the C-4′ carbon atom of the natural counterpart (*i.e.*, TBA-S_3 and TBA-S_{12}), it is not possible for both binding sites and TT loops to properly place at their thrombin whatever binding mode is assumed. Indeed,

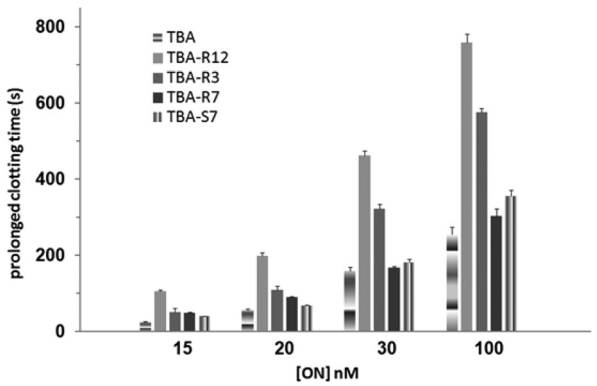

Fig. 6 Prolonged fibrinogen clotting time (s) in the presence of TBA or each active aptamer at different concentrations (15–100 nM). The graphics were drawn from scattering curve data.

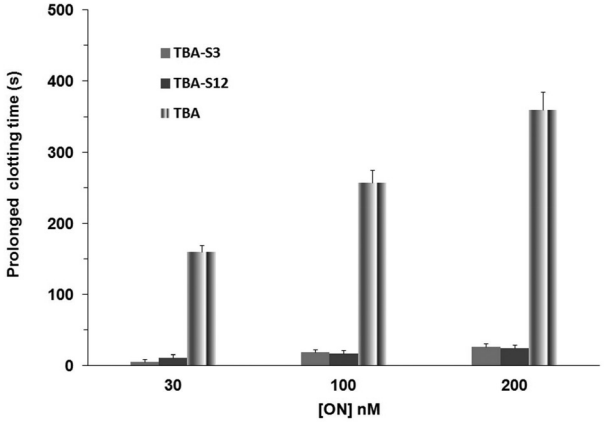

Fig. 7 Prolonged fibrinogen clotting time (s) in the presence of TBA, TBA-S_3, or TBA-S_{12} at different concentrations (30–200 nM). The graphics were drawn from scattering curve data.

Table 3 Prolonged fibrinogen clotting times of TBA and modified ONs. Each value was calculated subtracting the clotting time produced by thrombin in the absence of any inhibitor (*i.e.*, 25.6 ± 1.5 s) from that measured in the presence of the aptamer

	Prolonged clotting time (s)				
ON	15 nM	20 nM	30 nM	100 nM	200 nM
TBA	24.6 ± 2.7	56.4 ± 5.0	159.4 ± 11.3	256.4 ± 19.7	N.T.[a]
TBA-R_{12}	105.4 ± 5.7	198.9 ± 10.1	463.4 ± 13.6	759.6 ± 23.8	N.T.
TBA-R_3	50.4 ± 4.0	108.4 ± 5.1	323.4 ± 12.5	576.4 ± 22.8	N.T.
TBA-R_7	49.4 ± 3.0	89.4 ± 3.8	167.4 ± 6.0	304.4 ± 19.9	N.T.
TBA-S_7	39.5 ± 3.0	67.4 ± 4.0	181.4 ± 9.7	355.4 ± 18.0	N.T.
TBA-S_{12}	N.A.[b]	N.A.	10.9 ± 5.7	16.4 ± 2.8	24.4 ± 3.7
TBA-S_3	N.A.	N.A.	4.9 ± 3.0	18.4 ± 5.1	26.4 ± 4.6

[a] Not tested. [b] Not active.

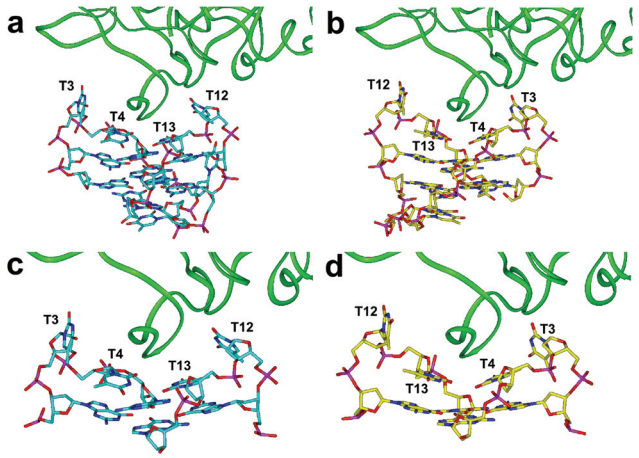

Fig. 8 X-ray structures of the complex between TBA and human α-thrombin presenting aptamer TT loops interacting with thrombin ABE I. (a) and (c) Binding mode III; PDB structure 1HAO (TBA carbons = cyan). (b) and (d) Binding mode IV; PDB structure 4DIH (TBA carbons = yellow). Heteroatoms are coloured as follows: O = red; N = blue; P = magenta. Thrombin ABE I is shown as a green ribbon.

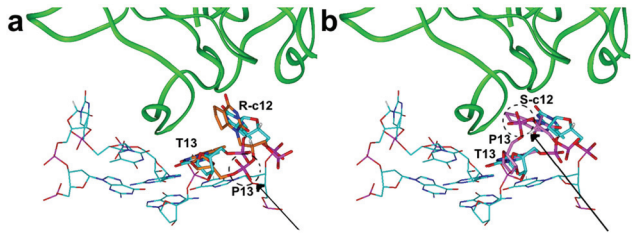

Fig. 9 (a) TBA-R_{12} (carbons = orange) and (b) TBA-S_{12} (carbons = pink) superimposed on the bioactive conformation of TBA in complex with thrombin (carbons = cyan; PDB ID: 1HAO). Heteroatoms are coloured as follows: O = red; N = blue; P = magenta. Thrombin ABE I is shown as a green ribbon. Hydrogens are omitted with the exception of those present in the modified residue chiral carbon (**R-c**12 and **S-c**12) and in TBA T12 C4′. The position of P13 is highlighted by a dashed circle and an arrow.

although monomers **c** are characterized by higher structural flexibility with respect to thymine, TT loop conformation is highly limited by the stacking of T4 and T13 on the G-quartet (Table S1 in ESI†). Therefore, when the nucleobase analogue moiety of **c** in TBA-S_3 and TBA-S_{12} projects in the same direction as the nucleobase of T3 and T12 in the bioactive conformation of TBA,[11,12,14] the succeeding phosphate group (*i.e.*, P4 or P13) is forced to distance itself from the G-quartet plane, likely causing steric clashes with the protein backbone (Fig. 9b).

Another important outcome which emerged from our results is the higher inhibitory activity of TBA-R_{12} compared to TBA-R_3.

In this case, the lack of structural symmetry does not explain the difference in activities of TBA-R_{12} and TBA-R_3, since the same TT loop binding mode at thrombin ABE I could be achieved for both analogues by rotating the structure by 180° (Fig. 8). This indicates that, although TT loops–ABE I interaction is necessary for biological activity, it is not the only

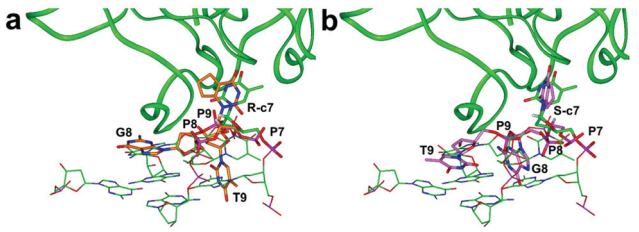

Fig. 10 (a) TBA-R_7 (carbons = orange) and (b) TBA-S_7 (carbons = pink) superimposed on the bioactive conformation of TBA in complex with thrombin (carbons = green; PDB ID: 1HAP). Heteroatoms are coloured as follows: O = red; N = blue; P = magenta. Thrombin ABE I is shown as a green ribbon. Hydrogens are omitted with the exception of those present in the modified residue chiral carbon (**R-c**12 and **S-c**12) and in TBA T7 C4′.

factor able to modulate the inhibition of thrombin. Further considerations can be done taking into account the results obtained with aptamers modified at position 7 of the TGT loop. The substitution of T7 with the *R* or *S* enantiomer of **c** produced almost equally active aptamers (Fig. 2 and Table 3). On the one hand, the lack of significant stereoselectivity of action between the two diastereomers would suggest that the TGT loop is not directly involved in thrombin binding. On the other hand, TBA-R_7 and TBA-S_7 showed increased inhibitory activity (either with respect to TBA and to previously developed analogues bearing the monomer **b**)[17] which cannot be ascribed to the increased stability of the quadruplex structure (T_m (PBS) TBA = TBA-T$_7$**b**[17] = 37.5 °C; TBA-R_7 = 38 °C; TBA-S_7 = 39 °C), thus supporting the possible direct involvement of the TGT loop in thrombin inhibition.[11,12,17,18] Our molecular modelling studies showed that, contrary to what was observed for the more rigid TT loops, the higher conformational flexibility of the TGT loop allows both **c** enantiomers to adopt the bioactive conformation[11,12] of the residue at position 7, without affecting the height of P7–P9 phosphate groups from the underlying G tetrad plane (Fig. 10). In particular, most TBA-R_7 conformers presented, similarly to TBA bioactive conformation, G8 stacked on the G1–G6–G10–G15 quartet and T9 pointing outside (Fig. 10a and Table S1 in ESI†).

The opposite trend was observed for TBA-S_7 (Fig. 10b and Table S1 in ESI†). Analyzing our results in the light of reported TBA–thrombin binding modes and X-ray structures,[11–14] it resulted that the two different TGT loop conformations can assume the binding modes I (Fig. S3a and S3c in ESI†) and II (Fig. S3b and S3d in ESI†) represented in Fig. 3.

Taken together, our results indicate that both TT loops and the TGT loop are involved in thrombin inhibition, but play different roles. The TT loops are necessary for high affinity thrombin inhibition by establishing a stereoselective interaction with the protein through residues at positions 3 and 12. In contrast, the TGT loop seems to be involved in less specific interactions with thrombin. Indeed, the TGT loop is not sufficient for significant thrombin binding when the binding ability of the TT loops is impaired (TBA-S_3 and TBA-S_{12}). Moreover, no significant stereoselectivity of action was observed between TBA-R_7 and TBA-S_7. The results of our molecular

modelling studies suggest that the flexibility of the TGT loop, together with the availability of multiple aptamer-protein binding modes, likely contributes to the observed lack of stereoselectivity between TBA-S_7 and TBA-R_7. Anyway, a single modification of the TGT loop at position 7 can enhance thrombin inhibition, through a still undefined molecular mechanism. A fascinating hypothesis, supported by some available X-ray data,[11,12] is that the high affinity binding of the TT loops could drive the interaction of the TGT loop with a second unit of thrombin, and this, in turn, due to thrombin allostery, somehow favours the binding of another TBA monomer in a cooperative mechanism.

Experimental

Materials and methods

Chemicals and anhydrous solvents were purchased from Fluka-Sigma-Aldrich. TLCs were run on Merck silica gel 60 F254 plates. Silica gel chromatography was performed using Merck silica gel 60 (0.063–0.200 mm). The API 2000 (Applied Biosystems) mass spectrometer was used to perform the analyses of the intermediates and the monomer. Melting points of intermediates **R-c** and **S-c** were measured using a Buchi Melting Point B-540. NMR experiments were recorded using Varian Mercury Plus 400 MHz and Unity Inova 500 MHz spectrometers and processed using the Varian VNMR software package. NMR spectra were calibrated using the solvents' residual proton or carbon signals as internal standards. ^{31}P-NMR spectra were calibrated using triphenylphosphine as an external standard (δ −6 ppm). Reagents and phosphoramidites for DNA syntheses were purchased from Glenn Research. ON syntheses were performed on a PerSeptive Biosystem Expedite DNA synthesizer. HPLC analyses and purifications were carried out using a JASCO PU-2089 Plus HPLC pump equipped with a JASCO BS-997-01 UV detector. CD experiments were performed on a JASCO 715 spectropolarimeter equipped with a PTC-348 temperature controller. The fibrinogen assay was performed using a JASCO 530 UV spectrophotometer equipped with the PTC-348 temperature controller. $[\alpha]_D^{20}$ values for **R-c** and **S-c** were determined using a JASCO P-2000 polarimeter. Molecular modelling calculations were performed on SGI Origin 200 8XR12000 and E4 Server Twin 2× Dual Xeon 5520, equipped with two nodes. Each node was 2× Intel Xeon Quad-Core E5520, 2.26 GHz, 36 GB RAM. The molecular modelling graphics were carried out on SGI Octane 2 workstations. MALDI-ToF measurements were performed using a Voyager DE-STR instrument (Applied Biosystems). High resolution mass spectra of **5a** and **5b** were performed on a Thermo LTQ Orbitrap XL mass spectrometer (ESI positive mode).

Synthesis procedure

Synthesis of monomers 5a and 5b

*6,7-Dihydro-1H-cyclopenta[d]pyrimidine-2,4(3H,5H)-dione (**1**).* **1** was obtained as previously reported by Takaya *et al.*[21] Briefly, a solution of ethyl-2-oxocyclopentanecarboxylate (10 g, 64.0 mmol), urea (5.76 g, 96 mmol) and HCl (37% w/w, 0.096 mL) in EtOH (20 mL) was refluxed for 3 h. After filtration, the collected white solid was suspended in 5% NaOH (24 mL) and refluxed for 1 h. The reaction was cooled to room temperature and the solid **1** collected by filtration and dried (yields 60%; R_f 0.42 in 9 : 1 CH_2Cl_2–CH_3OH, v/v).

^{1}H (400 MHz, mixture of CD_3OD and $CDCl_3$): δ 4.00 (bs, 2H), 3.62 (m, 4H), 3.03 (t, J = 7.3 Hz, 2H), 2.67 (t, J = 7.3 Hz, 2H), 2.10 (q, J = 7.3 Hz, 2H).

^{13}C (400 MHz, mixture of CD_3OD and $CDCl_3$): δ 166.3, 155.2, 147.3, 113.4, 34.8, 30.5, 18.0.

ESI mass (positive mode): calculated 152.1; found 153.1 $[M + H]^+$, 175.1 $[M + Na]^+$.

*1-(2,3-Dihydroxypropyl)-6,7-dihydro-1H-cyclopenta[d]pyrimidine-2,4(3H,5H)-dione [**S-c** or **R-c**].*[20] A mixture of compound **1** (1.0 g, 6.6 mmol) and anhydrous potassium carbonate (0.152 g, 1.1 mmol) in dry DMF (24 mL) was heated at 80 °C for 5 min. Compound **2** (pure enantiomer *R* or *S*) (0.490 g, 6.6 mmol) was then added. The reaction mixture was stirred at 80 °C for 18 h under argon. The solution was concentrated under reduced pressure and the residue purified by column chromatography on silica gel eluted with 90 : 10 CH_2Cl_2–CH_3OH to give **S-c** or **R-c** as white solids (yields **S-c** 45%, **R-c** 60%, each of them calculated as the average of two different reactions). Fig. S1† reports the CD profiles of each pure enantiomer **S-c** or **R-c**.

S-c ^{1}H NMR (400 MHz, pyridine-d_5): δ 4.66 (m, 1H, CHOH), 4.45 (dd, 1H, J_1 = 14.0 Hz, J_2 = 3.6 Hz, C*Ha*HbOH), 4.08 (d, 2H, J = 5.2 Hz, CH_2N), 3.93 (dd, 1H, J_1 = 14.0 Hz, J_2 = 8.6 Hz CHa*Hb*OH), 3.17 (m, 1H, C*Ha*Hb), 2.83 (m, 1H, CHa*Hb*), 2.69 (m, 2H, CH_2), 1.82 (m, 2H) (Fig. S4†).

S-c ^{13}C NMR (100 MHz, CD_3OD): δ 163.0, 160.4, 153.2, 111.6, 69.4, 63.9, 32.6, 27.0, 21.0 (Fig. S5†).

ESI mass (positive mode): calculated 226.1; found 227.1 $[M + H]^+$, 249.1 $[M + Na]^+$. $[\alpha]_D^{20}$ = –51.4.

S-c in the crystalline state was obtained from CH_3COCH_3–CH_3OH (99 : 1, v : v). The measured melting point was in the range 141–143 °C.

R-c ^{1}H NMR (400 MHz, pyridine-d_5): δ 4.66 (m, 1H, CHOH), 4.45 (dd, 1H, J_1 = 14.0 Hz, J_2 = 3.6 Hz, C*Ha*HbOH), 4.08 (d, 2H, J = 5.2 Hz, CH_2N), 3.93 (dd, 1H, J_1 = 14.0 Hz, J_2 = 8.6 Hz CHa*Hb*OH), 3.17 (m, 1H, C*Ha*Hb), 2.83 (m, 1H, CHa*Hb*), 2.69 (m, 2H, CH_2), 1.82 (m, 2H) (Fig. S6†).

R-c ^{13}C NMR (100 MHz, CD_3OD) 163.0, 160.4, 153.2, 111.6, 69.4, 63.9, 32.6, 27.0, 21.0 (Fig. S7†).

ESI mass (positive mode): calculated 226.1; found 227.1 $[M + H]^+$, 249.1 $[M + Na]^+$. $[\alpha]_D^{20}$ = +54.3.

R-c in the crystalline state was obtained from CH_3COCH_3–CH_3OH (99 : 1, v : v). The measured melting point was in the range 141–143 °C.

*1-(2,4-Dioxo-3,4,6,7-tetrahydro-2H-cyclopenta[d]pyrimidin-1(5H)-yl)-3-((3-methoxyphenyl)(4-methoxyphenyl)(phenyl)methoxy)-propan-2-yl-P-2-cyanoethyl-N,N-cianopropylphosphonamidate **5a** and **5b**.* Compounds **R-c** or **S-c** (560 mg, 2.5 mmol), 4,4′-dimethoxytrityl chloride (850 mg, 2.5 mmol) and 4-dimethylaminopyridine (15.0 mg, 0.12 mmol) were dissolved in dry pyridine (20 mL). The resulting solution was stirred at room

temperature under argon for 1.5 h. Dry methanol (200 μL) was then added to quench the reaction. After 30 min under stirring the solution was concentrated under reduced pressure and the residue purified by column chromatography on silica gel (eluted with 95 : 5 : 1 CH_2Cl_2–CH_3OH–Et_3N) to give mono-dimethoxytritylated derivative **4a** or **4b** as a white foam (1.16 g, 85% yield from each **c** stereoisomer; R_f 0.7 eluted with CH_2Cl_2–CH_3OH 95 : 5 v/v). The solid (859 mg, 1.6 mmol) was dried in a vacuum overnight before being dissolved in anhydrous DCM (9 mL) and diisopropylethylamine (1.7 mL, 10 mmol) under argon. 536 μL of β-cyanoethyl diisopropyl-chlorophosphoramidite was then added (2.4 mmol). After 40 min the reaction was quenched by addition of dry methanol (100 μL), diluted with ethyl acetate (15 mL) and finally washed with 10% sodium carbonate solution (15 mL) and brine (15 mL). The organic layer was dried on magnesium sulphate and concentrated in a vacuum. The residue was purified by silica gel chromatography eluted with *n*-hexane, ethyl acetate, and triethylamine (80 : 10 : 10). The fractions containing the product were collected and concentrated under vacuum yielding the phosphoramidite building block **5a** [from **R-c**] or **5b** [from **S-c**] as a white foam (1.05 g, 90% R_f 0.75 in $CHCl_3$–MeOH–TEA 97 : 3 : 0.05 v/v). HPLC chromatograms (Fig. S14 and S15†) were used to confirm yields of the conversions of **4a** and **4b** to **5a** and **5b**. After the washing procedure, the concentrated organic layers were dissolved in DCM and analyzed on a Hypersil silica gel column, particle size 5 μm, eluted with 50 : 50 *n*-hexane–ethyl acetate. R_t: **5a** 15.1 and **5b** 14.7 [min]. The yields of reactions, calculated as the ratio between the area of the peak produced by **5a** or **5b** and the total area of peaks, were 92 and 89%, respectively.

^{1}H NMR (500 MHz, DMSO-D6): δ 11.05 (1H), 7.41–7.24 (9H), 6.87 (4H), 4.18 (m, 1H), 3.93 (m, 1H), 3.78 (s, 6H), 3.78–3.40 (m, 3H), 3.14–2.85 (m, 3H), 2.65 (m, 1H), 2.49 (m, 4H), 1.92 (m, 2H), 1.08–0.97 (m, 12H) (Fig. S8 and S9†).

^{13}C-NMR (100 MHz, DMSO-D6): δ 162.0, 159.0, 158.6, 153.0, 145.5, 136.2, 130.5, 128.7, 128.5, 127.5, 119.5, 114.0, 111.5, 86.4, 70,6, 65.2, 59,0, 55.9, 49.0, 43.3, 32.9, 28.0, 25.2–24.9, 21.2, 20.5 (Fig. S10 and S11†).

^{31}P-NMR (202 MHz, DMSO): δ 148.9, 148.2 (Fig. S12 and S13†).

HR-ESI mass (positive mode): calculated 728.3339; found 751.3216 $[M + Na]^+$. Results of mass spectra are shown in Fig. S16 and S17.†

5a $[\alpha]_D^{20}$ = +55.3 (solvent CH_3CN); **5b** $[\alpha]_D^{20}$ = −45.7 (solvent CH_3CN).

Synthesis of oligomers. TBA and analogues were synthesized using standard solid phase DNA chemistry on a controlled pore glass (CPG) support following the β-cyanoethyl phosphoramidite method. The oligomers were detached from the support and deprotected by treatment with an aqueous ammonia solution (33%) at 55 °C overnight. The combined filtrates and washings were concentrated under reduced pressure, dissolved in H_2O, and purified by HPLC using an anionic exchange column eluted with a linear gradient (from 0% to 100% B in 30 min) of phosphate buffer at pH 7.0 (A: 20 mM NaH_2PO_4 aqueous solution containing 20% CH_3CN; B: 1.0 M NaCl, 20 mM NaH_2PO_4 aqueous solution containing 20% CH_3CN, elution time 15.3 min). The oligomers were successively desalted by molecular exclusion chromatography on Biogel P-2 Fine. The purity was checked on HPLC using an analytical reverse phase column (Purosphere RP-18, Merck). Finally, the sequences were analyzed in negative mode by MALDI-TOF experiments. Calculated molecular weight: [4710.25]; measured molecular weight: TBA-R_3 [4710.72]; TBA-R_7 [4710.94]; TBA-R_{12} [4710.54]; TBA-S_3 [4710.11]; TBA-S_7 [4711.57]; TBA-S_{12} [4710.72].

The concentrations of the samples used in CD and UV experiments were determined by measuring the absorbance at 260 nm at 80 °C and using the open access program available on http://basic.northwestern.edu/biotools/OligoCalc.html.[22]

CD experiments

To perform the CD experiments on modified nucleosides **R-c** and **S-c** each compound was dissolved in CH_3OH at the final concentration of 3.6×10^{-4} M. The two solutions were equilibrated for 10 min at r.t. and then the CD spectra were registered.

To perform the CD experiments on modified TBA sequences, each ON was dissolved in the potassium (90 mM KCl, 10 mM KH_2PO_4, pH 7.4) or PBS (90 mM KCl, 10 mM KH_2PO_4, pH 7.4) phosphate buffer at the final ON concentration of 2.0×10^{-5} M and submitted to the annealing procedure (heating at 90 °C and slowly cooling at r.t.). Before each experiment the samples were equilibrated at 10 °C for 30 min. CD spectra were recorded from 200 to 400 nm at 100 nm min^{-1} scanning rate, 16 s response, 1.0 nm bandwidth. Each CD profile was obtained by taking the average of three scans from which the spectrum of the background buffer was subtracted.

CD melting–folding curves were obtained by monitoring the variation of absorbance at 295 nm from 10 to 90 °C and *vice versa* in K^+ phosphate buffer (80 mM KCl, 20 mM KH_2PO_4 pH = 7.4) and PBS (147 mM NaCl, 20 mM NaH_2PO_4, 23 mM KCl, pH = 7.4) at [ON] = 2.0×10^{-5} M using a 1.0 cm cuvette. Two melting–folding experiments for each ON were recorded at 0.5 °C min^{-1} and 1.0 °C min^{-1} heating–cooling rate. No substantial differences between melting and cooling curves were detected. Both types of curves were independent of temperature scanning rate (0.5 °C min^{-1} or 1.0 °C min^{-1}). Fig. S2† shows the melting curves registered at the temperature scanning rate of 1.0 °C min^{-1}.

Fibrinogen clotting assay

The fibrinogen clotting times were measured spectrophotometrically.[23] ONs were incubated for 1 min at 37 °C in 1.0 mL of PBS containing 2.0 mg mL^{-1} of fibrinogen (fibrinogen from human plasma, F 3879, Sigma-Aldrich) in a PMMA cuvette (vol. 1.5 mL, c.o. 1 cm, Brand). 100 μL of human thrombin (10 NIH per mL; Sigma-Aldrich, T8885, human thrombin suitable for the thrombin time test) was then added to the solution containing the fibrinogen and the ON. The time required

for fibrin polymerization was determined from the UV scattering curve, registered as a function of time (wavelength fixed at 380 nm) in the presence of each ON. Each curve was determined in triplicate at different concentrations. The clotting time value reported as M ± SE was derived as the maximum of the second derivative of each scattering curve. The basal clotting time was determined by measuring the UV scattering as a function of time produced in the absence of any ONs. The 15-mer GTGTGTGTGTTGTGT was used as the negative control. In the absence of any inhibitor, the clotting time value was 25.6 ± 1.5 s. The prolonged fibrinogen clotting times of TBA and modified ONs were calculated by subtracting the clotting time produced by thrombin in the absence of any inhibitor from that measured in the presence of the aptamer.

Molecular modelling

Experimentally determined structures of TBA alone (PDB ID: 148D) and in complex with thrombin (PDB IDs: 1HAO, 1HAP, 1HUT, 4DIH, and 4DII) were downloaded from the Protein Data Bank (PDB, http://www.rcsb.org/pdb/) and analyzed using the Homology module of Insight 2005 (Accelrys Software Inc., San Diego, CA). Hydrogens were added to all these structures considering a pH value of 7.4 (Biopolymer Module, Insight 2005).

Since the replacement of T3, T7 and T12 residues with nucleoside **c** produced diastereomers characterized by *S* or *R* configuration at the acyclic linker, for each new TBA analogue, the two diastereomers were built by modifying the experimentally determined structure of TBA in complex with thrombin (PDB ID: 1HAO; Insight 2005 Builder module). Atomic potentials and charges were assigned using the CVFF force field.[24]

The conformational space of the new modified analogues was sampled through 200 cycles of simulated annealing (SA) followed by molecular mechanics (MM) energy minimization. During the SA procedure, the temperature is altered in time increments from an initial temperature to a final temperature by adjusting the kinetic energy of the structure (by rescaling the velocities of the atoms). The following protocol was applied: the system was heated to 1000 K over 2000 fs (time step of 1.0 fs); a temperature of 1000 K was applied to the system for 2000 fs (time step of 1.0 fs) to surmount torsional barriers; successively, the temperature was linearly reduced to 300 K in 1000 fs (time step of 1.0 fs). Resulting conformations were then subjected to MM energy minimization within Insight 2005 Discover_3 module (CVFF force field) until the maximum rms derivative was less than 0.001 kcal $Å^{-1}$, using a conjugate gradient[25] as the minimization algorithm. In order to reproduce the physiological environment where these molecules act and to evaluate the effects of the implicit solvent, we sampled the conformational space through the combined procedure of SA/MM calculations, using the dielectric constant of water ($\varepsilon = 80r$). Moreover, in order to allow a complete relaxation of the structures preserving the monomolecular chair-like G-quadruplex folding topology, during the entire course of SA/MM calculations, we applied a tether force of 100 kcal $Å^{-2}$ to the guanine bases of the two quartets.

Resulting conformers were analyzed and loop nucleotides were classified on the basis of: (i) glycosidic bond χ values, *i.e.*, $0° < \chi < 90° = syn$; $-60° < \chi < -180° = anti$;[26] $90° < \chi < 180°$ and $-60° < \chi < 0°$ = s/a; (ii) the interatomic distance between the centroid of the ring atoms of the nucleobase of each loop nucleotide and the centroid of the ring atoms of the nucleobases of the two G-tetrads (Pseudo_Atom Define command, Biopolymer Module, Insight 2005). When the distance was <8 Å, the loop nucleotide was classified as "stacked"; when the distance was >12 Å it was classified as "not-stacked". A 3D visual inspection was used to classify the nucleotide when the distance was included between 8 Å and 12 Å. In any case, a "stacked" nucleotide presented at least one nucleobase atom under the G-tetrads. Occurrence rates were calculated for all conformers (Tables S1 and S2 in ESI†).

New modified TBA conformers, resulting from SA/MM calculations, were superimposed on the experimentally determined structures of TBA in complex with thrombin (PDB IDs: 1HAO, 1HAP, 1HUT, 4DIH and 4DII) by fitting heavy atoms of the guanine bases of two quartets, and the overlap with the residues interacting with thrombin ABE I was evaluated. All possible TBA binding modes (Fig. 3) were considered. For each aptamer/enzyme complex a subset around the ligand including all protein and water molecules having at least one atom within a 6 Å radius from any given aptamer atom was defined. The created subsets were displayed and analyzed using Insight 2005 Biopolymer and Homology modules (Accelrys Software Inc., San Diego, CA).

Conclusions

The results presented herein clearly establish the role of loop conformational preferences on the overall TBA–thrombin complexes and illustrate how a stereochemical modification can impact on aptamer-protein recognition. Furthermore, since T residues are often loop components of aptamers, our analyses can be widely reproduced in other cases, using the *R*/*S* nucleoside derivatives **c** as two simple alternatives for the T residue, to acquire and/or refine the structure–activity relationship between aptamers and their targets.

Acknowledgements

This work was funded by the Italian MIUR grant FIRB RBFR12WB3W_003 (M.P.).

Notes and references

1 A. D. Keefe, S. Pai and A. Ellington, *Nat. Rev. Drug Discovery*, 2010, **9**, 537.
2 P. S. Pendergrast, H. N. Marsh, D. Grate, J. M. Healy and M. Stanton, *J. Biomol. Technol.*, 2005, **16**, 224.

3 D. Musumeci, G. Oliviero, G. N. Roviello, E. M. Bucci and G. Piccialli, *Bioconjugate Chem.*, 2012, **23**, 382.
4 D. Musumeci and D. Montesarchio, *Pharmacol. Ther.*, 2012, **136**, 202.
5 R. E. Wang, H. Wu, Y. Niu and J. Cai, *Curr. Med. Chem.*, 2011, **18**, 4126.
6 C. L. Esposito, S. Catuogno, V. de Franciscis and L. Cerchia, *Discovery Med.*, 2011, **11**, 487.
7 L. C. Bock, L. C. Griffin, J. A. Latham, E. H. Vermaas and J. J. Toole, *Nature*, 1992, **355**, 564.
8 P. Schultze, R. F. Macaya and J. Feigon, *J. Mol. Biol.*, 1994, **235**, 1532.
9 K. Y. Wang, S. H. Krawczyk, N. Bischofberger, S. Swaminathan and P. H. Bolton, *Biochemistry*, 1993, **32**, 11285.
10 W.-X. Li, A. V. Kaplan, G. W. Grant, J. J. Toole and L. L. K. Leun, *Blood*, 1994, **83**, 677.
11 K. Padmanabhan, K. P. Padmanabhan, J. D. Ferrara, J. E. Sadler and A. Tulinsky, *J. Biol. Chem.*, 1993, **268**, 17651.
12 K. Padmanabhan and A. Tulinsky, *Acta Crystallogr., Sect. D: Biol. Crystallogr.*, 1996, **52**, 272.
13 J. A. Kelly, J. Feigon and T. O. Yeates, *J. Mol. Biol.*, 1996, **256**, 417.
14 I. Russo Krauss, A. Merlino, A. Randazzo, E. Novellino, L. Mazzarella and F. Sica, *Nucleic Acids Res.*, 2012, **40**, 8119.
15 A. Avino, C. Fabrega, M. Tintore and R. Eritja, *Curr. Pharm. Des.*, 2012, **18**, 2036 and references cited therein.
16 T. Coppola, M. Varra, G. Oliviero, A. Galeone, G. D'Isa, L. Mayol, E. Morelli, M. R. Bucci, V. Vellecco, G. Cirino and N. Borbone, *Bioorg. Med. Chem.*, 2008, **16**, 8244.
17 N. Borbone, M. Bucci, G. Oliviero, E. Morelli, J. Amato, V. D'Atri, S. D'Errico, V. Vellecco, G. Cirino, G. Piccialli, C. Fattorusso, M. Varra, L. Mayol, M. Persico and M. Scuotto, *J. Med. Chem.*, 2012, **55**, 10716.
18 A. Pasternak, F. J. Hernandez, L. M. Rasmussen, B. Vester and J. Wengel, *Nucleic Acids Res.*, 2011, **39**, 1155.
19 T. B. Jensen, J. R. Henriksen, B. E. Rasmussen, L. M. Rasmussen, T. L. Andresen, J. Wengel and A. Pasternak, *Bioorg. Med. Chem.*, 2011, **19**, 4739.
20 T. Horhota, J. W. Szostak and L. W. McLaughlin, *Org. Lett.*, 2006, **8**, 5345.
21 T. Takaya, H. Yoshimoto and E. Imoto, *Bull. Chem. Soc. Jpn.*, 1967, **40**, 2844.
22 W. A. Kibbe, *Nucleic Acids Res.*, 2007, **35**(suppl.2), W43.
23 Y. R. De Cristofaro and E. Di Cera, *J. Protein Chem.*, 1991, **10**, 455.
24 P. Dauber-Osguthorpe, V. A. Roberts, D. J. Osguthorpe, J. Wolff, M. Genest and A. T. Hagler, *Proteins*, 1988, **4**, 31.
25 R. Fletcher, in *Practical Methods of Optimization*, John Wiley & Sons, New York, 1980, vol. 1.
26 (*a*) S. Neidle, *Principles of nucleic acid structures*, Academic Press, London, 2008; (*b*) J. Reichert and J. Sühnel, *Nucleic Acids Res.*, 2002, **30**, 253.

